The Ice Crystal–Graupel Collision Charging Mechanism of Thunderstorm Electrification

PETER BERDEKLIS AND ROLAND LIST

Department of Physics, University of Toronto, Toronto, Ontario, Canada

(Manuscript received 28 June 1999, in final form 2 November 2000)

ABSTRACT

The ice crystal–graupel collision charging mechanism, which is considered important in thunderstorm electrification, was studied using the newly developed Triple Interaction Facility that allows independent control of the solid, liquid, and vapor phases of a simulated cloud.

The advanced experiment led to the discovery of a new, dominant effect on charge transfer: the effect of relative humidity at which the ice crystals grow. It exceeds the impact of temperature and liquid water content (LWC). Higher relative humidity (close to water saturation) always promoted stronger negative charging, while lower humidity (close to ice saturation) led to weaker negative or stronger positive charging. The effect was greatest at temperatures of around $-15°C \pm 3°C$. Newly established was also a velocity dependence on charging with a maximum at relative graupel–air speed of ~ 5 m s^{-1}.

The reversal temperature, previously considered to be unique at a given LWC, was found to be also a function of the relative humidity (RH). Now, changes in RH can explain quantitatively the differences between once controversial observations of previous investigators.

A parameterization of the results is presented for use in numerical thunderstorm models, and a new conceptual model of thunderstorm electrification is suggested.

1. Introduction

The ice crystal–graupel collision charging mechanism of thunderstorm electrification, also known as noninductive precipitation charging, is based on the experimental observation that a charge transfer occurs when ice crystals collide with simulated graupel particles within a cloud of supercooled water droplets. A relatively large body of laboratory data has made this concept the most widely accepted, even if there are no clear physical explanations.

The three cloud chamber studies forming the foundation of the ice crystal–graupel collision charging theory (Reynolds et al. 1957; Takahashi 1978; Jayaratne et al. 1983) used target particles that were rotated in a mixed phase cloud of ice crystals and supercooled water droplets. Significant charging during collisions with ice crystals only occurred when supercooled water droplets were present. The sign and magnitude of the charge transfer was found to be a function of temperature and liquid water content (LWC), but substantial disagreement exists and has not been resolved.

Reynolds et al. (1957) observed that the sign of the charge transfer to the target changed from negative to positive as the concentration of ice crystals was raised from between 10^2 and 10^5 L^{-1} to between 10^4 and 10^6 L^{-1}, an observation largely ignored in the other studies.

Takahashi (1978) measured the charge transfer over a wide range of cloud temperatures and LWC and found that for a fixed LWC the sign of the charge transfer changed from positive to negative, at the so-called reversal temperature, as the temperature was lowered. This temperature was a function of the LWC.

Jayaratne et al. (1983) found that the reversal temperature rather varied with the effective liquid water content (ELWC; mass fraction of water accreted by the target). Accounting for differences in LWC and ELWC, the pattern of reversal temperatures observed by Jayaratne et al. (1983) and Takahashi (1978) differ significantly. Furthermore, the maximum charge transfers observed by Takahashi were up to two orders of magnitude greater than those observed by Jayaratne et al.

The work of Jayaratne et al. (1983) has been extended in the intervening years by the ''Manchester group,'' which has consistently reported results that support their original findings. Among other things, this group has shown that the charge transfer to the target is also a function of target particle velocity and ice crystal size (Keith and Saunders 1990), but none of the findings have explained the difference between the charging patterns observed by Takahashi (1978) and by Jayaratne et al. (1983). Numerical models of thunderstorm elec-

Corresponding author address: Professor Roland List, Department of Physics, University of Toronto, Toronto, ON M5S 1A7, Canada. E-mail: list@atmosp.physics.utoronto.ca

trification also suggest that, unless very high precipitation rates are present, the charge transfer observed by the Manchester group is too weak to account for the observed rapid development of thunderstorm electric fields (Dye et al. 1986).

Recently the Manchester group attempted to recreate the experiments of Takahashi (1978). They suggested that the difference between the observed charge transfers was due to different ways of measuring the cloud LWC (Brooks and Saunders 1995). Takahashi has not accepted this argument, and has recently reproduced his original results (Takahashi 1999).

In addition to differences in experimental observations, no consistent theory of the physics underlying the charge transfer has been established despite more than 40 yr of laboratory studies, and the ice crystal–graupel collision theory has long been a focus of criticism (Mason 1988; Vonnegut et al. 1995). Saunders (1995) suggested in his review that a competition between two or more mechanisms may provide the observed charging pattern. Thus, a need for new and different laboratory studies became evident.

2. The Triple Interaction Facility (TIF) measurements, procedures, and performance

a. The icing tunnel and control variables

Unlike cloud chambers, the TIF (Fig. 1), first described by Berdeklis and List (1996), is capable of producing a stable cloud composed of independently controlled ice crystals, supercooled water droplets, water vapor, and graupel. The facility consists of an icing wind tunnel (List et al. 1987), connected to an ice crystal growing chamber (ICC), and a measuring system.

The wind tunnel has been used for over a decade to study the growth and the heat and mass transfer of graupel and hailstones (Zheng and List 1996; Greenan and List 1995; Cober and List 1993; Garcia-Garcia and List 1986; Lesins and List 1986). It has an airtight closed circuit that can be pumped down to pressures as low as 30 kPa. For the current experiments the wind tunnel was configured to simulate graupel growth at laboratory pressure (Cober 1991).

A centrifugal fan ([1], Fig. 1; all square brackets refer to Fig. 1) created an updraft in the measuring section of 3–7 m s^{-1}. This corresponds approximately to the fall speeds of 3–5-mm-diameter graupel at cloud altitudes (Locatelli and Hobbs 1974; List and Schemenauer 1971). The airspeed was monitored by a pressure transducer [13] across the 12-fold contraction [12] below the measuring section. A 100-point average was converted into an airspeed, accurate to ± 0.1 m s^{-1} and recorded at 3 Hz (Fig. 2a).

Temperature control to -30°C was provided by combining the action of a refrigeration unit [5] and three heaters [2]. A combination of wall flaps [7] and a perforated wooden board [8] reduced the airspeed in the measuring section and increased speed and cooling in the outer square-ring of the double-walled tunnel [14a and 14b]. This led to a very homogeneous temperature in the inner part of the measuring section. A shielded copper–constantan thermocouple [14] recorded 100-point average temperatures at 3 Hz with an accuracy of ± 0.1°C. At temperatures above -6°C the tunnel temperature could be kept constant to within ± 0.3°C, and to less than ± 0.1°C at lower temperatures. Typical measuring section temperatures are shown in Fig. 2b.

A spray nozzle, located 2 m below the riming target [11], produced a droplet cloud with an LWC between 0.2 and 2.0 g m^{-3} by varying the nozzle water flow rate. The droplet size distribution was changed by adjusting the nozzle airflow rate. Distilled, deionized water was used for all experiments. The nozzle assembly was heated to $<+8$°C, giving the cloud droplets sufficient time to cool to ambient temperatures before reaching the measuring section (Cober 1991).

The LWC of the cloud, W_f (g m^{-3}), was calculated from the nozzle water flow, F (g s^{-1}) using $W_f = F A^{-1} V^{-1}$, where A (m^2) is the cross section of the measuring section and V (m s^{-1}) the airspeed. This simple geometric analysis holds because of the uniform LWC distribution in the measuring section (Cober 1991) and the balance between ice deposits on the walls below the measuring section and the reduction of LWC in the 1-cm-thick boundary layer.

Cober (1991) measured the droplet size distribution for five different airflows (Table 1) using the magnesium oxide technique (May 1950; Cober 1987). The distributions were verified using a 10-μm resolution Particle Measuring System (PMS) Two-Dimensional Cloud Particle Greyscale Probe (2DCG; Berdeklis 1998). The ELWC is a measure of the mass fraction of liquid water accreted by a target when compared to the swept out volume LWC of a given cloud. The target collection efficiency was measured for the different droplet size distributions at a velocity of 5.0 m s^{-1} and an LWC of 0.99 g m^{-3} (Table 1).

Electrification of a droplet cloud is well known for droplet formation by breakup, as occurs by using spray nozzles (Iribarne 1972; Iribarne and Klemes 1974). The signature of droplet charging in the spray-produced tunnel cloud consisted of a high-frequency signal and a bias current (ice free phase in Fig. 3a). The first is caused by the randomness of the individual droplet charges and the high resolution of the measurement. The appreciable standard deviation, in this case $\sigma = \pm 3.5$ pA, is generally a function of droplet size distribution and ELWC. In the current experiment the standard error of the estimate of the bias (mean) current, determined using a 1-min baseline from 02:10 to 03:10 min (relative time, 179 measurements), was ± 0.26 pA. The bias current from the droplet charging was subtracted from the current associated with the ice phase (Fig. 3a). Thus, the current of the ice particles alone is established. The

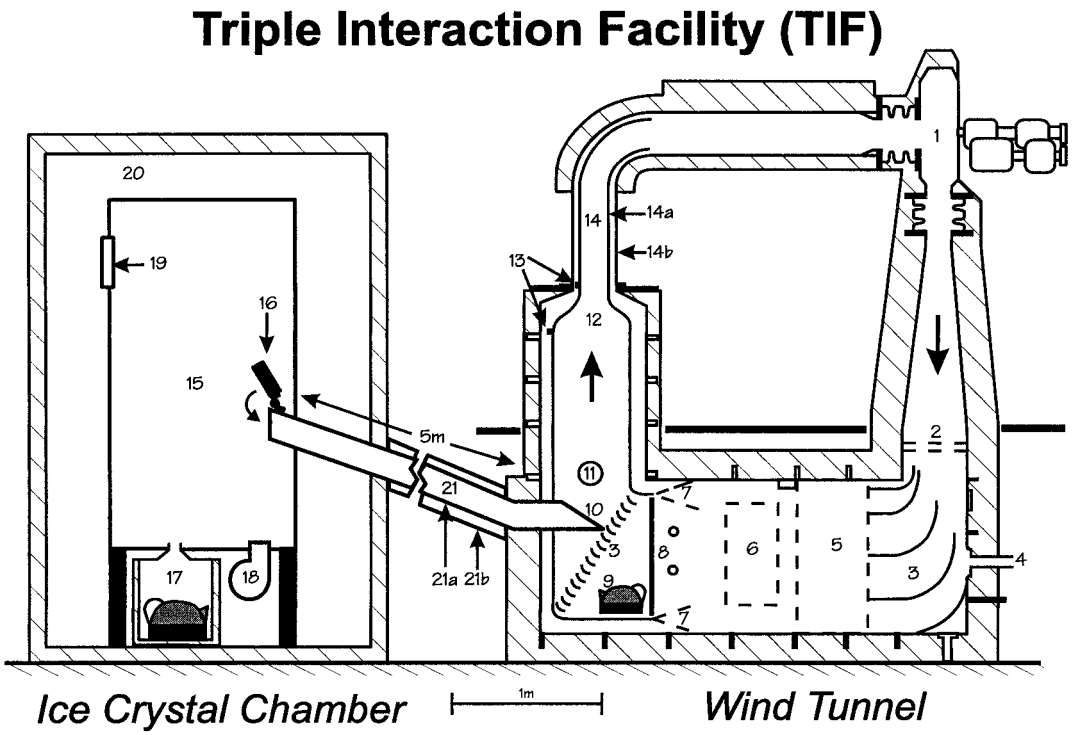

FIG. 1. The wind tunnel: [1] tunnel fan; [2] heaters; [3] turning vanes; [4] pipe to vacuum pump; [5] cooling element; [6] access door; [7] double wall flaps; [8] perforated wooden board; [9] tunnel kettle; [10] ice crystal injection; [11] water injection; [12] contraction; [13] pressure measuring nipples; [14] measuring section (a: inner wall, b: outer wall). The ice crystal chamber: [15] ice crystal growing chamber (ICC); [16] pipe access door; [17] steam kettle in insulated can; [18] chamber fan; [19] chamber window; [20] cold room; [21] connecting pipe (a: ice crystal pipe, b: dry ice pipe).

high-frequency variation of the droplet charging was treated as statistical error, specific for each experiment.

The tunnel relative humidity with respect to ice (RHI) is measured by the psychometric method using a second shielded, ice-coated thermocouple placed next to the thermocouple for the measuring section temperature. At a tunnel temperature of $-15°C$, $\pm 0.1°C$ (the accuracy of the two thermocouples) corresponds to $\pm 4.3\%$ RHI. Below $-15°C$, humidity measurements are less accurate. The humidities increased with increasing LWC and temperature from 100% to 109% RHI [109% equals 94% with respect to water (RHW)]. For future experiments, the tunnel RHI could be increased up to 140% RHW by placing a kettle in the tunnel [9], recognizing that the TIF measuring section is maintained at quasi-steady-state conditions and not at equilibrium.

b. The ice crystal chamber (ICC) and ice crystals

The ICC [15] for producing ice crystals had dimensions 1.22 m $\times$ 2.44 m $\times$ 2.39 m (7.1 m^3) and was set up in a walk-in freezer that could be cooled to $-25°C$. Typically, the chamber was kept within $\pm 3°C$ of the temperature of the wind tunnel. Exceptions were for the study of the effect of ice crystal shape, when temperatures differed by as much as 10°C.

The chamber was connected to the wind tunnel by a 5-m-long, 10-cm-diameter aluminum pipe [21a] that was surrounded by a second, 15-cm-diameter PVC pipe [21b] that was partially filled with dry ice pieces. The inner pipe entered the tunnel through an access port [10], 10 cm below the spray nozzle. Inside the ICC a lid controlled the transfer of the ICC air–ice crystal mixture to the tunnel [16]. The inner pipe temperature warmed throughout an experiment day from $-30°$ to $-8°C$.

A droplet cloud (steam) was produced in the ICC using an insulated kettle [17]. Ice crystals were initiated by briefly inserting a liquid nitrogen–cooled rod. The chamber fan [18] maintained a homogeneous temperature before and after experiments.

The ice crystal chamber relative humidity, (ICC RH) was classified qualitatively as low, intermediate, or high, depending on the density of the droplet cloud at the time of ice crystal initiation, as observed using a flash light. ''Wisps'' of steam, entrained within mostly clear air would result in ''low'' chamber humidity. After ice crystal initiation, a low RH cloud was composed mostly of ice crystals. An even distribution of steam throughout the chamber, but with good visibility through the steam, was classified as ''intermediate,'' that is, between ice and water saturation because water droplets and ice crystals were present in similar concentrations. ''High'' humidity was reached when the corners of the chamber opposite to the window were no longer visible because

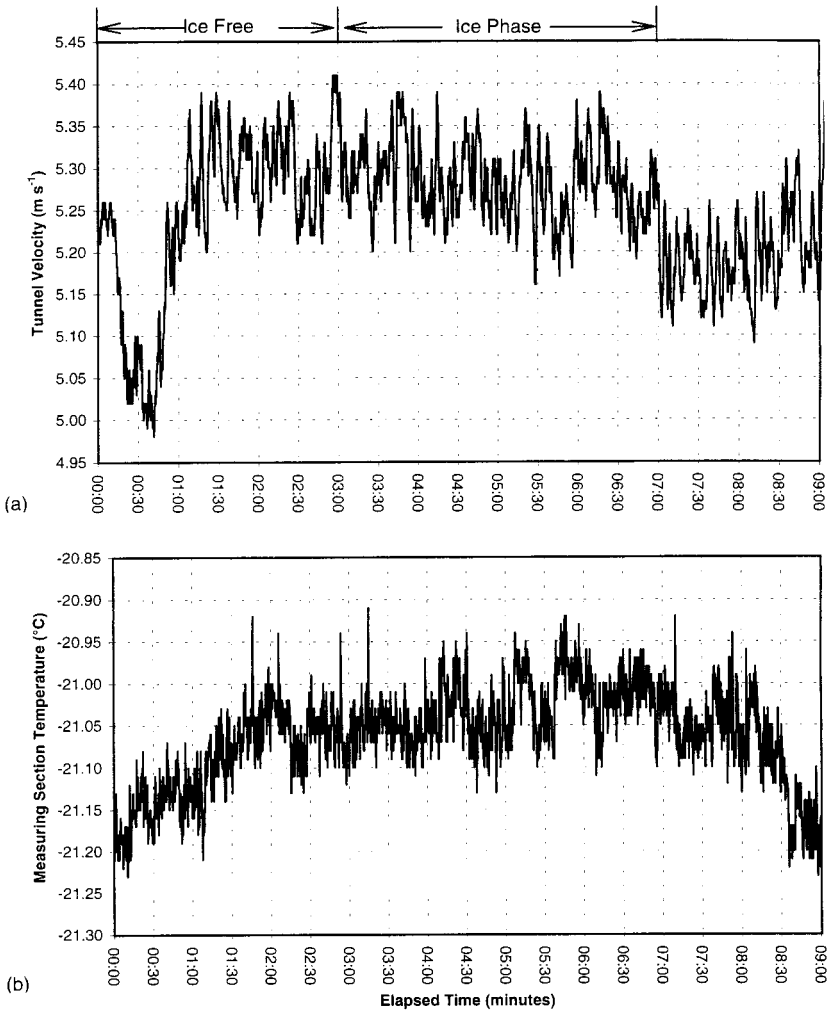

FIG. 2. Average temperature and velocity in the measuring section for baseline and ice phase 02:10–07:00 min.: −21.04 ± 0.04°C and 5.29 ± 0.05 m s^{-1}.

of a high droplet concentration and LWC. This overabundance of droplets would result in little degradation of the water saturation by the introduction of ice crystals.

A vacuum pump [4] continuously sucked ice crystals into the tunnel where they appeared 10–15 s after observation in the chamber. The ice crystal flow could be maintained for >6 min, although typical experiment runs lasted 2–4 min.

Ice crystal habits, sizes, and concentrations were determined by crystal collection at the bottom of the cloud chamber through formvar replication (Takahashi and Fukuta 1988), followed by observation under a microscope at room temperature. The habits varied with tem-

TABLE 1. Droplet size distribution.

Nozzle airflow rate [air] = mm	Mean droplet diameter [d] = μm	Mean volume diameter [d_v] = μm	Median volume diameter [d_m] = μm	Number of droplets measured	Target collection efficiency [%]
83.0 ± 0.5	19.2	21.8	24.6 ± 2.0	1396	34 ± 2
75.0	20.8	24.2	29.6	2485	39
68.0	23.0	27.0	34.8	1169	50
63.0	24.6	29.6	39.8	1296	61
61.0	24.8	30.2	42.0	735	51

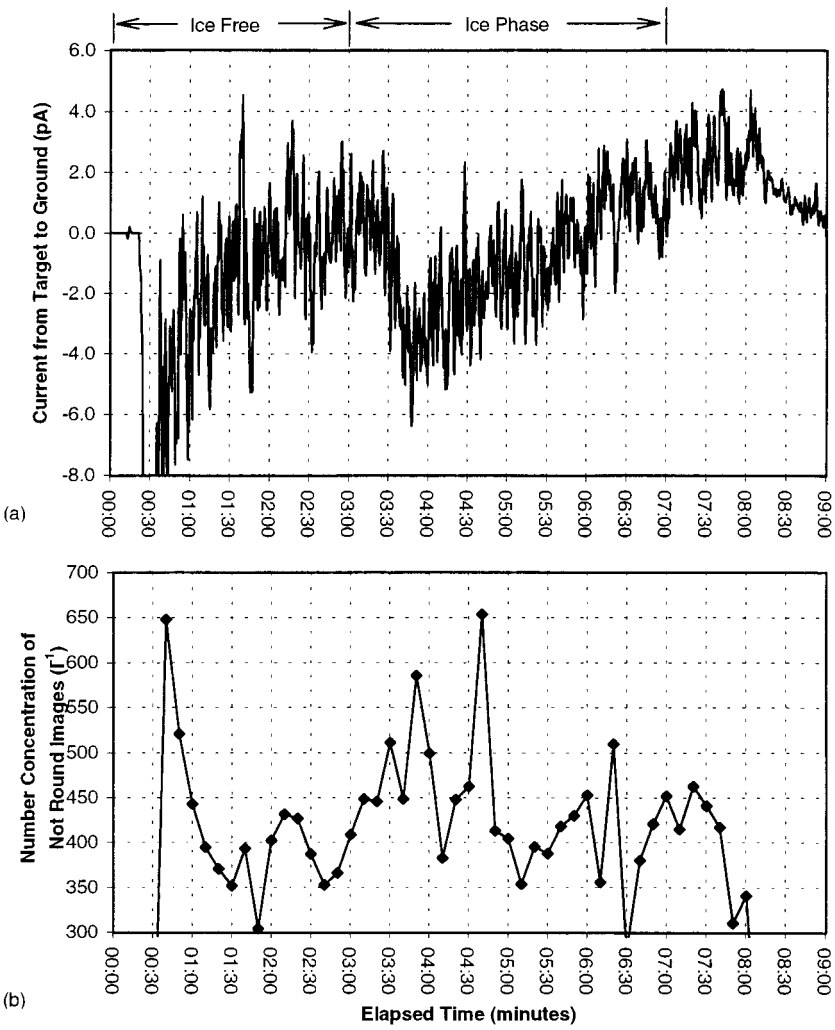

FIG. 3. Tunnel conditions as in Fig. 2. (a) Charging pattern; (b) 10-s average number concentration of ''not round'' images for experiment at -21°C, ELWC $= 0.56 \pm 0.006$ g m^{-3}, and velocity $V = 5.29 \pm 0.05$ m s^{-1}; for 20.8-μm mean diameter droplet distribution. Background current and number concentration calculated using baseline from 02:10 to 03:10 (min: sec relative time). Ice crystals initiation in ICC at 3:00 min, first observed at 3:10, and in measuring section in 03:30 and 03:40 min.

perature as described by Takahashi et al. (1990). At -8°C plates were predominant, at -16°C dendrites were observed. Ever present were triangular habits, as observed in high cirrus clouds below -40°C by Hallett (1997). Most ice crystals in the ICC were between 50 and 100 μm in size, with estimated concentrations $>10^4$ L^{-1}.

Ice crystal concentrations and sizes in the center of the measuring section are determined by a PMS 2DCG probe (resolution 10 μm, with a minimum detectable particle size of 40 μm). Crystals are distinguished from droplets by an algorithm distinguishing spherical versus other shapes. The method also had to account for droplets not appearing spherical due to technical realities. To establish the true ice particle concentration the number of the ''nonround'' droplets was determined during the ice-free phase (Fig. 3a) and subtracted from the overall total. From Fig. 3b a typical example of 10-s average ice crystal concentrations of 60–300 L^{-1} can be deduced. For this graph these figures have been corrected for the bias caused by the concentrations of nonround droplets of 403 ± 57 L^{-1} with a $\sigma = 23.3$ L^{-1} for six consecutive 10-s averages. Ice crystals of all size classes were present in any 10-s average.

c. Measuring section and measuring system

The measuring section ([14] and Fig. 4), where the target particle was suspended and observed, has a double aluminum wall with an inner cross section of 17.8 cm $\times$ 17.8 cm and a height of 70 cm. The walls act as a Faraday cage with little external electrical noise.

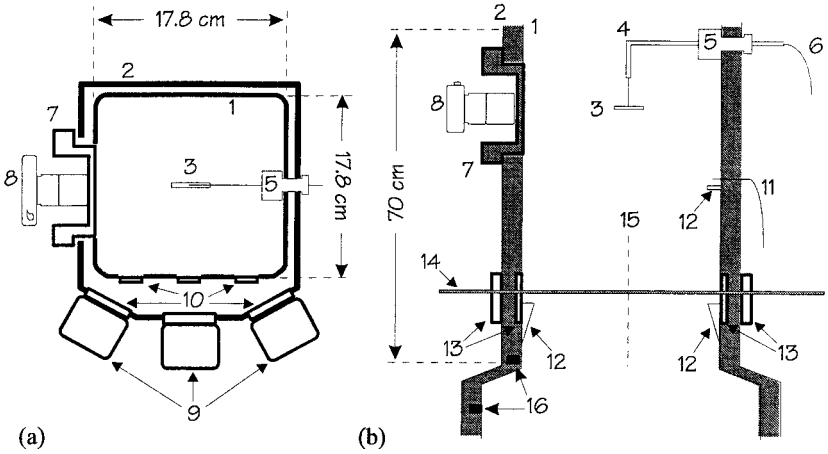

FIG. 4. (a) Horizontal and (b) vertical cross section of the wind tunnel measuring section: 1, inner walls; 2, outer walls; 3, target particle; 4, particle support; 5, Teflon collar; 6, low noise coaxial cable; 7, access door; 8, camera; 9, strobe lights; 10, strobe windows; 11, thermocouples; 12, riming shields; 13, 2DCG windows; 14, 2DCG laser beam; 15, 2DCG object plane; 16, pressure transducer nipples.

The photographic system consisted of 1) a Nikon F camera with a 55-mm micro lens and a Nikon M extension tube, with a depth-of-field of ~8 mm. Mounting was flush to the inner access door; 2) three strobe lights at 45°, 90°, and 135° from the camera axis. Droplets are observed using the 45° and 135° strobes, whereas ice crystals are best seen at 45° and 90°. Video equipment was also available.

A special PMS 2DCG laboratory probe with a 60 optical sensor array and an active beamwidth of 600 μm was used to determine number concentration and size distribution of wind tunnel cloud particles. Joe and List (1987) showed how the four grayscale levels could be used to determine the distance of an object from the focal plane. This allows accurate estimation of the sample volume specific for each size class and, thus, cloud particle concentrations (see also Berdeklis 1998). The image files for one experiment ranged from 3 to 25 Mb depending on the droplet size distribution, tunnel velocity, LWC, and duration of the experiment. The particle concentration and associated errors were established by calibration with glass beads.

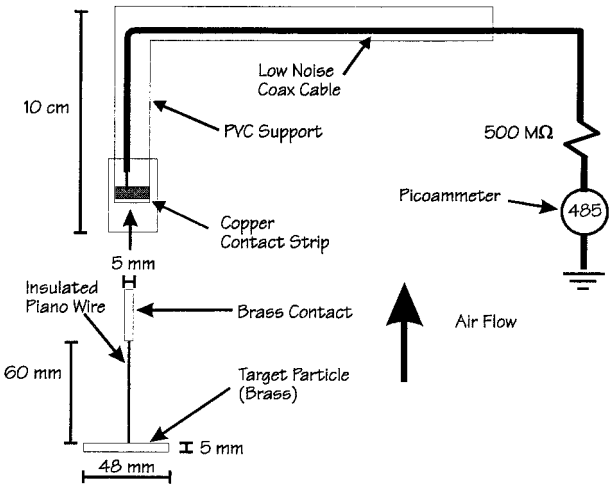

FIG. 5. Target particle and particle support. Cylindrical brass target (48 mm long, 5 mm diameter) simulates a graupel.

The estimated error of the number concentration for each ice crystal size bin was calculated for every 10-s average, assuming a Poisson distribution and estimated errors for the depth-of-field calibration (Berdeklis 1998). The error for the total number concentration was calculated from the error estimates for each size bin using standard error propagation analysis.

The target particle suspension device in the measuring section (Fig. 5) housed a low-noise coaxial cable for the charging measurement. The cylindrical target particle (length 48 mm, diameter 5 mm) was similar to those used in cloud chamber experiments of other authors. It was chosen over a graupel-shaped target because the swept-out volume is larger, providing a higher charging current that was easier to measure.

The support was anchored to the inner wall of the measuring section (Figs. 4 and 5). A 5-cm-diameter Teflon collar prevented rime ice from forming a second electrical path to ground. The coaxial cable connected the target to ground through a 500-MΩ resistor and a calibrated Keithley 4 1/2 digit, ±20 000 count picoammeter, model 485 {resolution 0.1 pA, 3-Hz readings, accuracy ±[0.4% of the reading +4 counts (0.4 pA)], 100-point averages}. With no cloud in the measuring section the noise was typically ±0.1 pA. This corresponds to a potential difference of 50 mV between target and ground.

Ten-second average current-to-ground values were calculated, during the same 10 s as used for number concentration. For each point the average charge trans-

fer per ice crystal collision Q was calculated using $Q = I(A\ V\ N)^{-1}$, where I is the average current-to-ground minus the mean bias current, A is the cross-sectional area of the target particle (2.4 cm^2), V is the tunnel velocity averaged from the beginning of the (ice-free) baseline until the end of the ice phase, and N is the number concentration minus the mean bias concentration of nonround droplets. The error for each estimate was calculated using standard error propagation analysis.

Each experiment was performed at fixed ICC and tunnel temperatures, airspeed, LWC, and droplet size distribution. All experiments on any given day were performed at the same tunnel and chamber temperatures and care was taken to maintain close to identical initial conditions. A typical time sequence of major events in the experiments is reflected in Figs. 2 and 3, assuring that proper stabilities and equilibria had been achieved.

3. Results

a. Experimental range and general observations

The temperature in the measuring section ranged from -5°C to -21°C; LWC's from 0.25 to 2.0 g m^{-3} and velocities from 3 to 6 m s^{-1}, with most series run at $\sim$5 m s^{-1}. Five droplet size distributions were used with mean droplet diameters of 19.2, 20.8, 24.8, 24.6, and 23.0 μm, although most series used only the first three. ICC RH ranged from ice saturation to water saturation. A total of 172 experiments were performed, producing a data file totalling 2–3 Gb. The results are presented with associated errors, representing one standard deviation from the mean.

Note that no adjustment was made to the estimated charge transfer to account for the collision efficiency established at less than unity for ice particles <80 μm by Keith and Saunders (1988). However, the errors associated with experimental estimates of the collision efficiency are very high and, therefore, would add little to the analysis. Consequently, the collision efficiency for the case at hand was set to unity. Thus, the actual charge transferred to the target during an ice crystal collision could be systematically greater than suggested by these experiments.

A common feature of the experiments performed at intermediate to high ICC humidities was that the charge transfers estimated from data points within 30–60 s of the beginning of the ice phase were always much more negative than those at later stages, as shown for the test experiment of Fig. 3. The average charge transfer per collision Q from the 10-s intervals beginning at 03:30, 03:50, and 04:00 min were -14 ± 10, -17 ± 7, and -18 ± 14 fC per ice crystal collision, respectively. The charge transfer calculated at 04:40 min is -4.1 ± 2.0 fC per collision. This reduction is caused by the depletion of the water vapor in the ICC by the growing ice crystals, favoring more positive charging. Despite this behavior, the average charge transfers were calculated (Berdeklis 1998) using all charge transfer estimates made within the ice phase of an experiment, except where noted. This leads to another systematic underestimate of the charge transfer at high relative humidities that is not accounted for in the error analysis.

The final estimate of Q was determined by taking the weighted average of the 10-s estimates. Only points with number concentrations near to or greater than the estimated concentration error are included in the average. Lower concentrations have much larger associated charge transfer errors, larger than the estimated charge transfer, and so have little influence on the weighted average. The number of points used for the weighted average varied between experiments from 1 to 17, although 4 to 8 was typical. The standard deviation associated with the weighted average is equal to the square root of the inverse of the sum of the weights (Mandel 1964). In the current experiment the final estimate was $Q = 5.5 \pm 1.9$ fC per collision, using the four data points listed above.

Note that all charge transfer estimates were made using 10-s intervals. Using different intervals in the analysis may lead to somewhat different estimates. Note also that all findings and statements are only considered valid within the experimental ranges covered.

b. Results of the experimental series

The experimental series revealed dependencies of the charge transfer on droplet size distribution, temperature, ELWC, ICC RH, and velocity. Note that, except where indicated, ICC RH was ''intermediate,'' that is, between ice and water saturation, and the velocity was fixed at $\sim$5 m s^{-1}.

The series also revealed no dependence of the charging on the temperatures of the ICC or of the connecting pipe. Temperatures in the ICC were typically within ± 3°C of those of the wind tunnel. However, experiments were performed in which the temperatures differed by up to 10°C. Again, no measurable dependence on ICC temperature was observed. Similarly, connecting pipe temperatures varied from -30° to -8°C during an experiment day. Experiments repeated with only the pipe temperature changed showed no observable dependence on pipe temperature. These facts will be important for the physical interpretation of charging effects.

The effect of droplet size distribution was studied in experiments at fixed LWC over a range 0.25–2.0 g m^{-3}, but for three droplet size distributions with mean droplet diameters of 19.2, 20.8, and 24.8 μm. Figure 6a shows that Q at -21°C and similar LWCs varies with the droplet distribution. For the 24.8- and 20.8-μm distributions the maximum charge transfer occurs at a LWC of 1.0 and 1.4 g m^{-3}, respectively; for 19.2 μm two peaks of Q occur at 0.5 and 1.5 g m^{-3}. Figure 6b shows the same results, this time plotted against the ELWC. The peak of Q corresponds to an ELWC of approximately 0.55 g

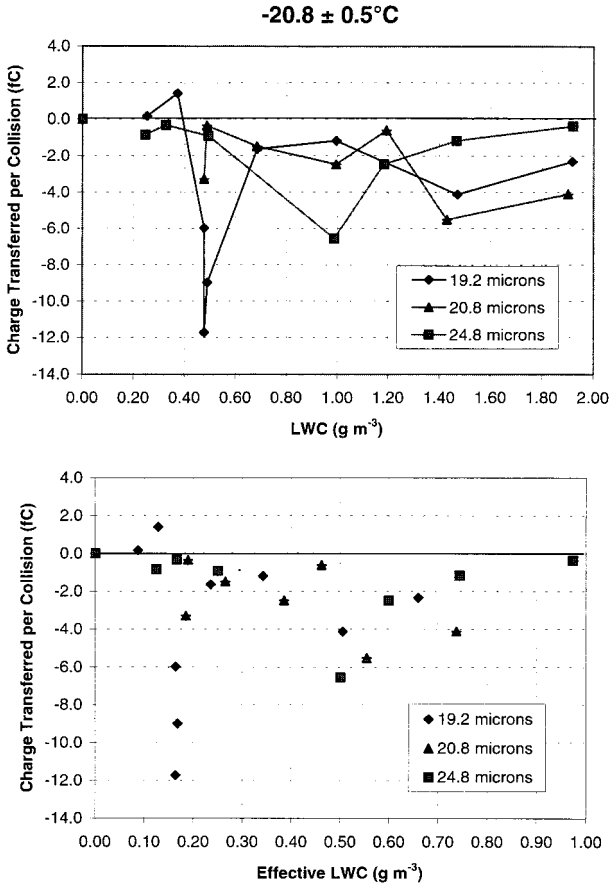

FIG. 6. (a) Charge transferred per collision for three droplet size distributions, for LWCs between 0.25 and 1.9 g m^{-3}; (b) same data against better fitting (effective) ELWC.

m^{-3} for all three distributions. The relationship between Q and ELWC holds well throughout the range, except for the sharp spike at ELWC of 0.16 g m^{-3} for the 19.2-μm distribution peak at 0.48 g m^{-3} LWC. This spike is the result of variations in ICC RH (see below). In light of the more pronounced dependence of Q on ELWC, rather than on LWC, the following data will be displayed accordingly.

The effect of temperature and ELWC was measured at $-5°$, $-8°$, $-11°$, $-14°$, $-16°$, $-18°$, and $-21°$C (Figs. 6–9). For fixed ELWC the magnitude and sign of the charge transfer is a function of temperature. Above $-10°$C the charge transferred to the riming target is positive at all ELWCs. Below $-16°$C the charge transfer is always negative. The temperature of the sign reversal moves to higher temperatures with increasing ELWC. The sharp spikes at $-16°$C (ELWC = 0.33 g m^{-3}) and at $-21°$C, and the large variability between experiments at $-14°$C and $-16°$C (ELWCs 0.5–0.6 g m^{-3}) are effects of variations in ICC RH.

The effect of ICC RH on the sign and magnitude of the Q was quite dramatic and unexpected. Figure 10 shows that at low chamber humidity weak positive charging was observed, while strong negative charging occurred at high chamber humidity. Details of the charging patterns and measuring section RH are shown in Fig. 11 for an experiment at low ICC RH (near ice saturation) and for high ICC RH (near water saturation) in Fig. 12. Both experiments were performed under identical tunnel conditions. In both cases the measuring section relative humidity was approximately 103% of ice saturation. Note that the bias current observed during the ice-free phase needs to be subtracted from the total current of the ice phase to determine Q. Figure 13 shows an experiment performed under the same tunnel conditions as Figs. 11 and 12, but at intermediate RH. In this case the sign of the charge transfer to the target, with respect to the baseline, changed from positive to negative during the experiment as the steam in the chamber was depleted by the growing ice crystals. Similar sign change charging patterns were observed in two other intermediate relative humidity experiments at $-14°$C, 0.5 g m^{-3} ELWC using the 20.8-μm distribution and at $-15°$C, 0.5 g m^{-3} ELWC using the 24.8-μm distribution.

The average charge transfer to the target at a constant ELWC, as a function of temperature and ICC RH, is displayed in Fig. 14. At temperatures below $-10°$C relative humidities near water saturation always caused a stronger negative charge transfer than did humidities near ice saturation. Above $-10°$C humidities near water saturation weakened the positive charge transfer nearly to zero.

For each temperature the range of the minimum and maximum average charge transfers, corresponding to the highest and lowest relative humidities, is well defined. The greatest effect of the relative humidity was observed between $-13°$ and $-17°$C. Outside this temperature range charge transfers observed at high ICC RH differ by 2–8 fC per collision to those at low RH. Between $-13°$ and $-17°$C the range is between 20 and 25 fC per collision, and changes in sign of the transfer were often observed.

For the experiment shown in Fig. 12, estimates from 10-s intervals between 05:00 and 05:40 min suggest charge transfers per collision of $Q = -44 \pm 27$ fC, compared to -13 ± 7 fC averaged over the entire ice phase. Near $-16°$C maximum negative charge transfers greater than -60 fC per collision were observed near the start of the ice phase. Since these very strong charge transfers are very short lived phenomena, typically lasting much less than 1 min, these data are not shown in Fig. 14. They are also not represented in the range of charge transfers described by the ''envelope'' curves in Fig. 14. Only charge transfers averaged over the entire ice phase are shown, except where a sign change during an experiment was observed as in the experiment of Fig. 13.

Patterns similar to those shown in Fig. 14 occur at other EWLC and velocities values. In preliminary experiments (not shown), negative charging was observed

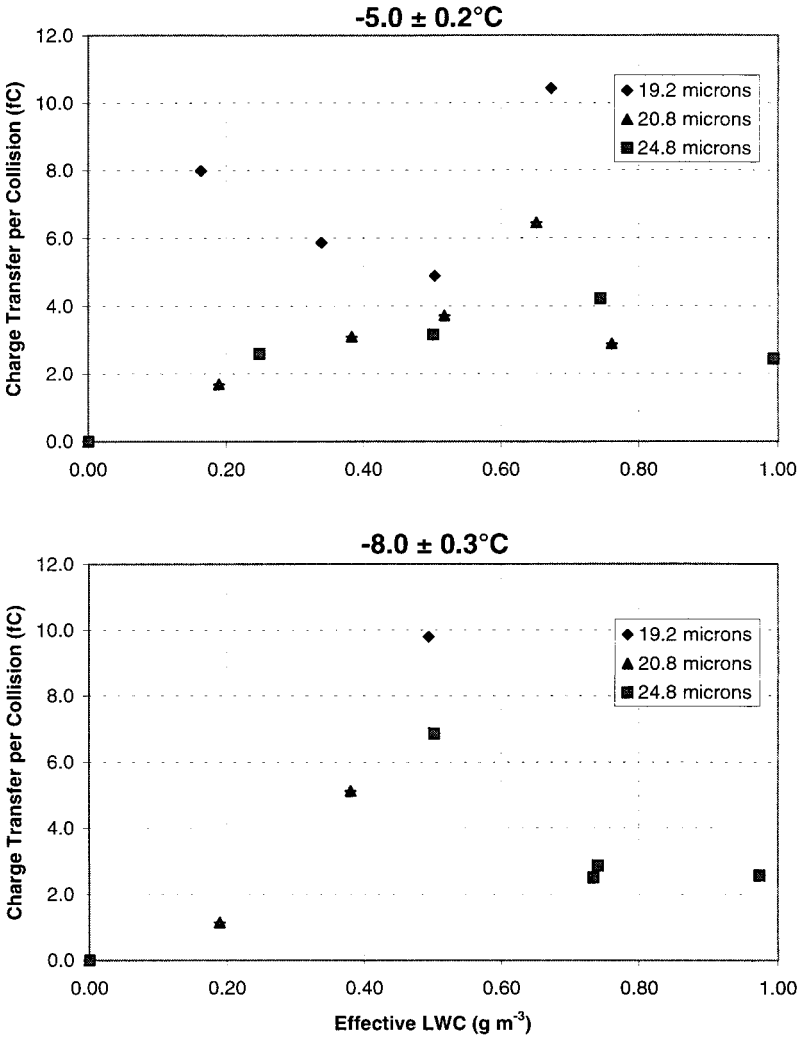

FIG. 7. Effect of temperature and ELWC on average charge transferred to riming target. At temperatures >-10°C: positive charge transferred at all ELWCs.

at -5.5°C and 4 m s^{-1}, and at -2.5°C and 3 m s^{-1} for high ICC RH and an ELWC of 0.7 g m^{-3}. Low ICC RH always caused the charge transfer to be more positive.

The effect of velocity on the charge transfer was measured at velocities of approximately 3, 4, 5, and 6 m s^{-1} (Fig. 15) under otherwise constant conditions of -16°C, 0.5 g m^{-3} ELWC, and high ICC RH. A weighted average negative charge transfer of -16 fC was observed at $\sim$5 m s^{-1} while at velocities of 3, 4, and 6 m s^{-1} the maximum negative charge transfer was much lower at ~-5 fC per collision. These observations are nearly 5 standard deviations apart. Time constraints did not permit further investigation of the effect of velocity.

4. Parameterizations of the average charge transfer per collision

The surface plot of the average charge transfer per ice crystal collision as a function of temperature and ELWC (Fig. 16a) was created using 134 of the 141 data points shown in Figs. 6–9, taken at a velocity of $\sim$5 m s^{-1}. Negative charge transfers stronger than -20 fC, observed in nine experiments performed at -16°C, were not included because they were carried out at high relative humidity. Figure 16b shows the surface plot of a polynomial fitted to the experimental data for intermediate ICC RH.

In order to parameterize the charge transfer per collision, Q, data were chosen and fitted at five constant ELWCs: 0.24 $\pm$ 0.05, 0.35 $\pm$ 0.05, 0.55 $\pm$ 0.05, 0.70 $\pm$ 0.05, and 0.98 $\pm$ 0.02 g m^{-3} by third-order polynomials as functions of temperature. Since data points at constant temperature and ELWC do not necessarily represent estimates of Q under identical RH conditions, an unweighted least squares method was used.

The coefficients of the five charge transfer versus temperature fits were then themselves fitted to third-order polynomials of ELWC. This technique resulted in

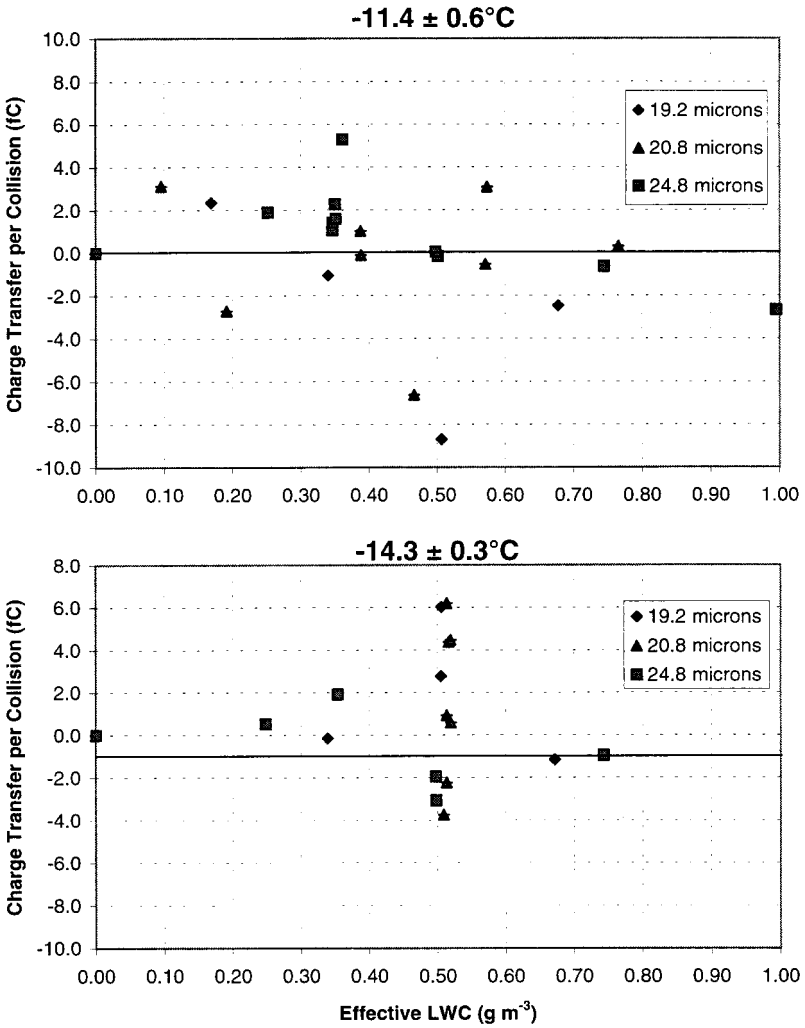

FIG. 8. Effect of temperature and ELWC on sign of charge transfer to the target; note change from positive to negative <-11°C for ELWCs >0.5 g m^{-3}. At -14°C strong sensitivity to RH in ICC, leading to scatter at 0.5 g m^{-3}.

much better agreement with the data, as measured using the χ^2 statistic, than by using the techniques by Press et al. (1992). The resulting function of charge transfer to the target, Q (fC) versus temperature, T (°C) and ELWC, E (g m^{-3}), is

$$\begin{aligned} Q = {} & (48.1645 - 363.697E + 760.679E^2 - 472.745E^3) \\ & + (17.0144 - 132.123E + 257.76E^2 \\ & \quad - 153.578E^3)T \\ & + (1.48765 - 11.8361E + 22.5847E^2 \\ & \quad - 13.4002E^3)T^2 \\ & + (0.03762 - 0.30446E + 0.578584E^2 \\ & \quad - 0.34597E^3)T^3. \end{aligned} \tag{1}$$

This parameterization is representative for temperatures between $-5°$ and -21°C, an ELWC between 0.1 and 1.0 g m^{-3}, and a velocity of 5 m s^{-1}.

It should be noted that the number of significant figures quoted in Eq. (1) does not indicate the accuracy of the model estimate. Rather, the precision of the parameterization is necessary to account for the order of magnitude range of the ELWC that is modeled. The accuracy of the model is indicated by the difference between the measured charge transfer and the model estimate (Fig. 17a). The largest errors occur at low ELWC where few data points were available and at -18°C where the model overestimates the negative charge transfer to the target. Large errors also occur at -15°C but these differences are due to the scatter of points caused by the sensitivity to the ICC RH. Figure 17b shows a histogram of the difference between the measured charge transfer and the model estimate for all 134 fitted points. Note

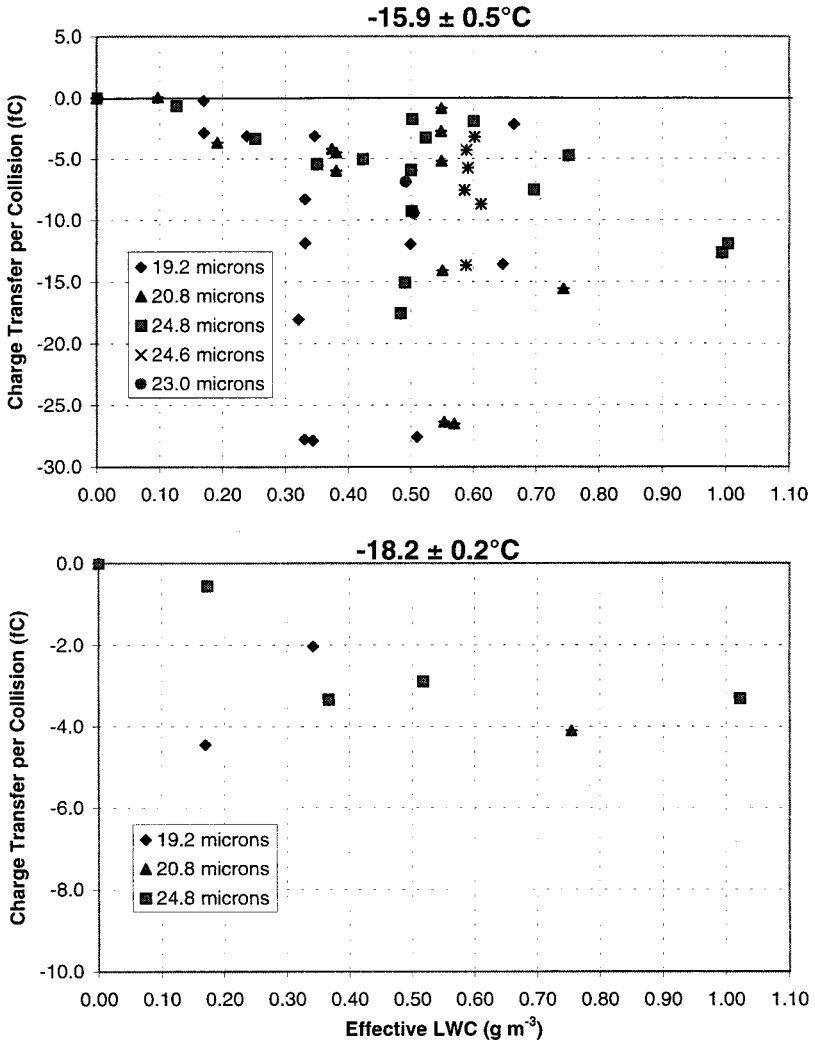

FIG. 9. Effect of temperature and ELWC: <-16°C charge transferred to target negative at all ELWCs. At -16°C large scatter of data indicative of very strong sensitivity to ICC RH. Series at -16°C includes two additional droplet distributions; results consistent with dependence of charging on ELWC.

that over 73% of the points are within ± 3 fC of the measured value.

The effect of the ICC RH is characterized by two curves that model the extremes of the charge transfers observed at the lowest and highest humidities (Fig. 14). These curves correspond to chamber relative humidities of ~100% RHI and ~100% RHW, respectively. The envelope of charging, Q_i [fC], near ice saturation, was fitted to a third-order polynomial function of temperature T [°C]

$$Q_i = -26.8771 - 9.03809T - 0.71137T^2 - 0.01604T^3. \quad (2)$$

For chamber humidities near water saturation the envelope of charging Q_w [fC] was fitted to a fourth-order polynomial of temperature

$$Q_w = -23.5666 - 3.4278T + 0.77055T^2 + 0.133107T^3 - 0.004448T^4. \quad (3)$$

Equations (2) and (3) are valid for an ELWC of 0.5 g m^{-3} at temperatures between $-5°$ and -19.5°C and for a velocity of 5 m s^{-1}. Equation (3) is a parameterization of the maximum observed negative charge transfer averaged over the entire ice phase of a high relative humidity experiment, rather than the maximum transfer observed in any subperiod.

As can be seen in Fig. 14, Eq. (2) provides good agreement with the most positive charge transfers ob-

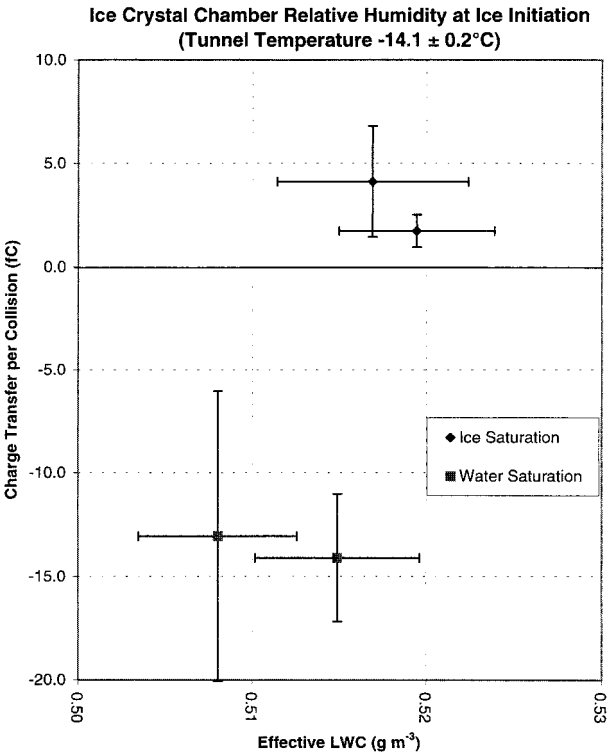

FIG. 10. Charge transfer for ICC near RHI and RHW at time of ice crystal initiation. Tunnel conditions -14.1 ± 0.2°C, 5.26 ± 0.03 m s^{-1}; for 20.8-μm mean diameter droplet distribution.

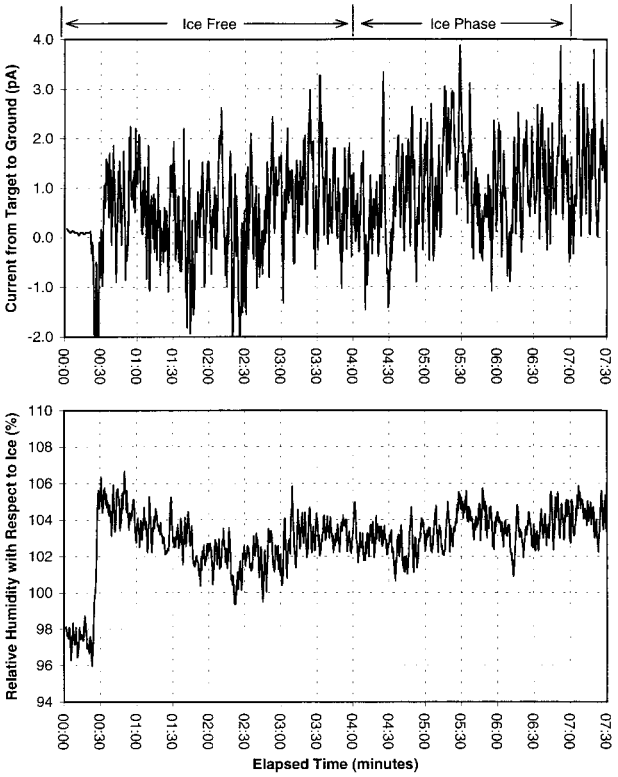

FIG. 11. Charging pattern and measuring section RH for ICC RH near ice saturation. Note related positive charge transfer with average $C = +4.4 \pm 2.3$ fC. Tunnel conditions: -14.3 ± 0.05°C; 5.28 ± 0.05 m s^{-1}; ELWC $= 0.52 \pm 0.005$ g m^{-3}.

served, while Eq. (3) shifts the strongest negative charge transfer from $-15°$ to -17°C. A lack of measured points does not warrant more detailed fits.

5. Discussion

a. The physics of the charge transfer

The dependence of the charge transfer on cloud conditions indicates that two or more properties of the colliding particles are involved (see review by Saunders 1993), properties that may be different for the riming targets and the vapor-grown ice crystals. The key effects that need explanation are displayed in the three experiments of Figs. 11–13, which were performed under identical tunnel conditions, that differed only in ICC RH. They showed a positive charge transfer at low RH, a negative one at high RH, and a sign change at intermediate RH. In all three cases RH in the measuring section of the icing tunnel was approximately 103% of ice saturation. The dependence of the charge transfer on the ICC RH, rather than the tunnel RH, suggests that the ice crystals have a ''memory'' of the growth conditions in the chamber, which lasts at least 10–15 s, the crystal travel time from chamber to measuring section. Further, any acceptable physical model must explain the *continuous* change in charging with changes in the ICC RH. The observation that the temperatures of the ICC and the connecting duct to the tunnel have no observed effect on charging is another clue.

A change in crystal habit could provide a memory effect. However, it is too abrupt for a gradual change in charging, particularly at -15°C (Hanajima 1949). Ice crystal (surface) temperature is also not a candidate because of the short thermal relaxation time. Height and growth rate of steps in the ice crystal surface could provide a long-term memory because they are continuous functions of humidity (Hobbs 1974). However, there are no reports in the literature of charge associated with steps.

A dislocation, defined by Hobbs (1974) as ''a line defect in a crystal that disrupts the otherwise ideal arrangement of the atoms or molecules'' was found to be proportional to the growth rate of ice crystals (Keith and Saunders 1990), and is known to carry positive charge density (Itigaki 1970, 1983). However, since charge carriers in ice are protons, the transfer of charge from ice crystals to the target would be more positive with increasing growth rates and could oppose the main RH dependence observed.

The quasi-liquid-like layer (QLL) of ice is a few mono-molecular layers thick. It is not considered normal liquid water because it exists in a steady-state balance with ice on the one side and vapor on the other (Hobbs

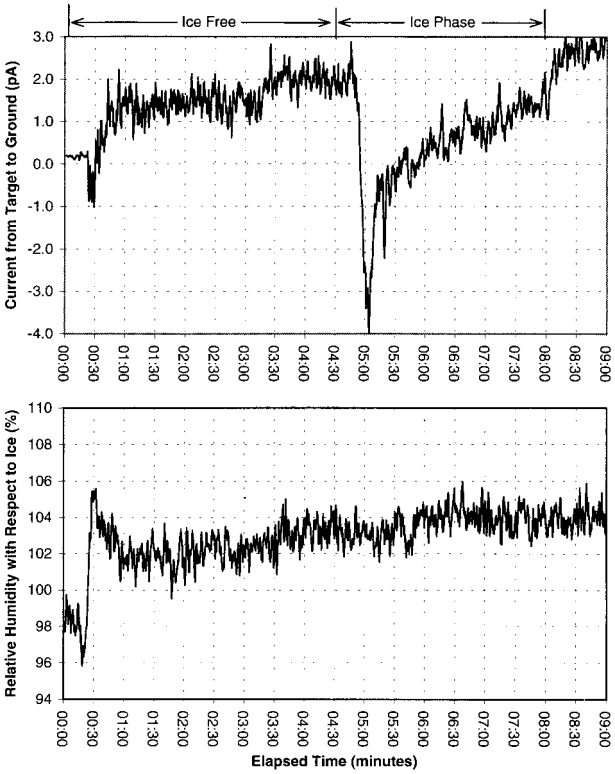

FIG. 12. Charging pattern and measuring section RH for ICC RH near water saturation. Note strongly negative charge transfer, with $C = -13.1 \pm 7.0$ fC. Tunnel conditions: -14.0 ± 0.01°C; 5.29 ± 0.04 m s^{-1}; ELWC $= 0.51 \pm 0.005$ g m^{-3}.

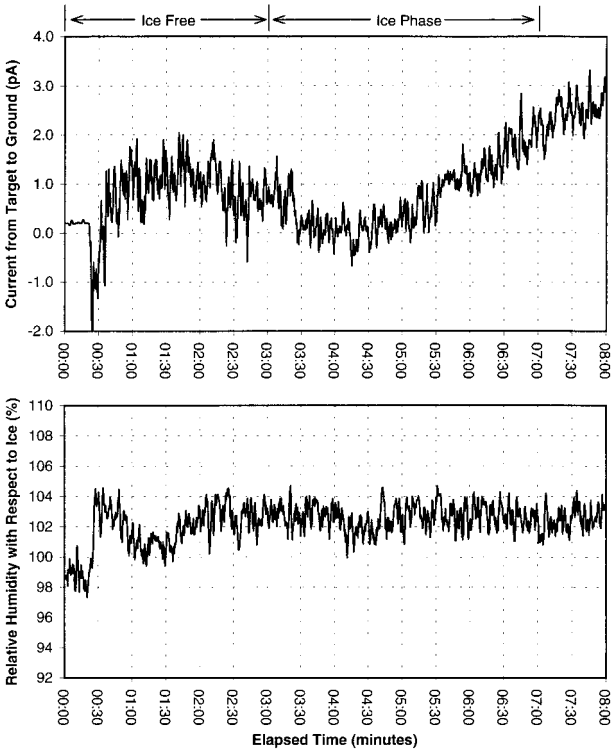

FIG. 13. Charging pattern and measuring section RH for intermediate ICC RH (between ice and water saturation), with sign change of charge transfer during experiment. Calculated average $C = -2.2 \pm 0.3$ fC from 03:20 to 05:31 min.; $C = +0.93 \pm 0.71$ fC from 5:31 to 6:11 min, and $C = +6.2 \pm 2.3$ fC from 6:11 to 7:00 min. Tunnel conditions: -14.2 ± 0.01°C; 5.23 ± 0.05 m s^{-1}; ELWC $= 0.51 \pm 0.005$ g m^{-3}.

1974) to temperatures as low as −30°C (Baker and Dash 1989). The thickness of the QLL is considered to be a function of ambient temperature and growth rate from the vapor, with higher temperatures and faster growth rates creating thicker layers (Baker and Dash 1989). At the liquid–vapor surface an electrical double layer may exist similar to the double layer observed at bulk water–vapor interfaces (Iribarne 1972) and provide an excess of negative ions. Baker and Dash (1989) proposed that charge transfer between colliding ice particles could be caused by fluid transfer between the QLLs, with negative charge moving from the double layer of the thicker QLL (faster growth) to the thinner. This property would be consistent with the observed dependence on RH. However, no estimates of the relaxation time are available to indicate if a QLL memory could last the required 10–15 s.

Competition between negative charging through QLL mass exchange and positive charging through differences in dislocation densities may explain the sign change presented in Fig. 13. An ice crystal that initially grows rapidly under intermediate to high RH enters the tunnel with a thick QLL and transfers negative charge to the target. As the humidity in the chamber drops, the thickness of the QLL is reduced but dislocations created during the initial rapid growth remain. When the QLL effect weakens the dislocation effect becomes dominant and positive charge is transferred to the target.

No other mechanism offered in the literature [contact potentials between rimed and unrimed surfaces (Caranti and Illingworth 1983); fracture of rime structures charged due to temperature gradients (Caranti et al. 1991)] can provide an explanation, and no other ice crystal properties are known at this time that change with relative humidity.

b. Dependence of the charge transfer on velocity

The collision velocity affects the particle contact time during which the charge transfer takes place. The longer the contact time, the more charge can be transferred between the QLLs of the ice particles. Therefore, lower velocities should transfer more charge. However, longer contact times may also allow a ''neutralizing current'' (Iribarne 1972) to develop across the contact point that would partially discharge the initial transfer. A neutralizing current is an essential feature of the theory of droplet charging. The competition between fluid transfer charging and the neutralizing current is a nonlinear function of contact time, perhaps with a preferred velocity of 5 m s^{-1}.

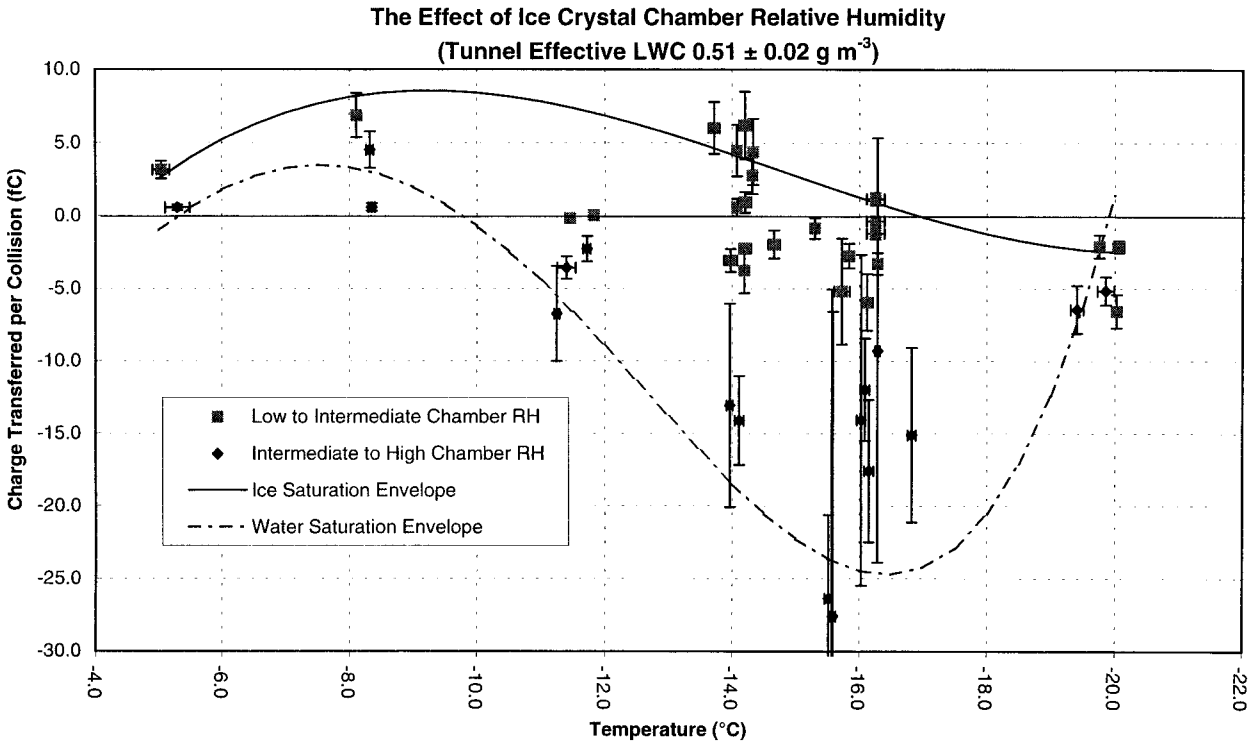

FIG. 14. Effect of ICC RH between water and ice saturation on C, at ELWC = 0.51 g m^{-3}, velocity 5.3 m s^{-1}, and constant temperature. Note that higher ICC RH promotes more negative charging. Ice and water saturation envelopes calculated from Eqs. (2) and (3), respectively.

There may be another cause. Graupel, defined as porous, dry ice particles, are rarely found in nature with sizes >5 mm. A possible reason is a surface area–specific diminishing of the heat and mass transfer, coupled with higher accretion rates, leading to a wetting of the particle surface and an ineffective charge transfer due to sticking and otherwise changed conditions.

6. Comparison with previous experimental studies

a. The effect of relative humidity

One of the greatest puzzles in the field of thunderstorm electrification has been the disagreement of the experimental results of Takahashi (1978) and Jayaratne et al. (1983). While both studies found that the charge transfer is a function of the cloud temperature and LWC, they differed in most other respects. Jayaratne et al. and the Manchester group have always argued that the charge transfer is a function of the ELWC rather than the LWC, and this is supported by the present results. However, even if the results of Takahashi are adjusted to an estimated ELWC for the droplet size distributions used, the charging pattern observed would still differ significantly from Jayaratne et al. The dependence of the charge transfer on the relative humidity may provide an explanation for the different reported charging patterns.

Figure 18 shows a comparison of the transfers reported by Takahashi (1978), the Manchester group, and Eq. (1) of the present work. The results of the Manchester group were calculated using equations presented in Saunders et al. (1991) and are adjusted for differences in velocity and ice crystal size according to the power-law dependence described in that work. The data for Takahashi (1978) were taken from his Fig. 8 with and without adjustment for velocity (Saunders et al. 1991), assuming that 1 g m^{-3} LWC was equivalent to 0.5 g m^{-3} ELWC. Figure 18 also shows the relative humidity envelopes of Fig. 14, calculated using Eqs. (2) and (3). With minor exceptions, all the charge transfers fall well within the relative humidity envelopes, suggesting that the different patterns are the result of the different humidity regimes.

The effect of relative humidity is a confirmation of the observation of Reynolds et al. (1957) that the sign of the charge transfer changed from negative to positive when the number concentration of ice crystals was increased to greater than that of the cloud droplets. This lowers the cloud chamber humidity toward ice saturation and promotes positive charging. When droplets outnumber ice crystals the humidity rises toward water saturation, promoting negative charging.

b. The velocity dependence of the charging

The unadjusted positive charge transfers observed by Takahashi (1978) are much higher than the maximum

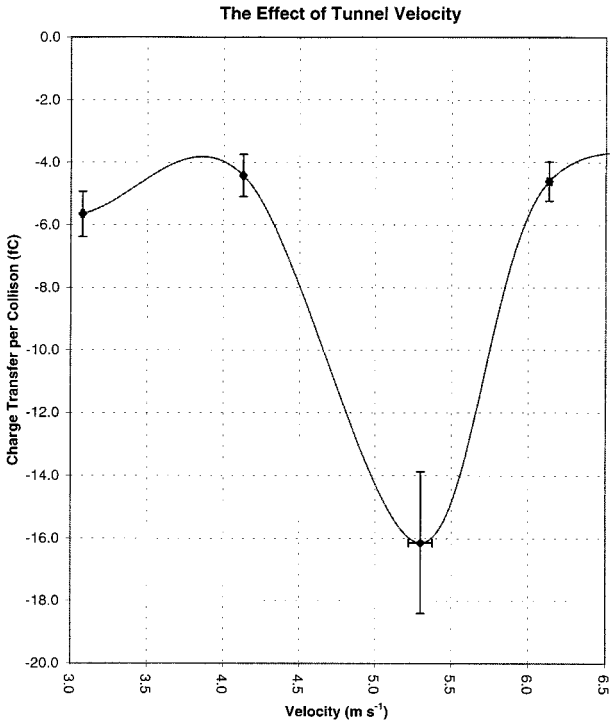

FIG. 15. Negative charge transfer as function of tunnel velocity; ICC at RHW. Data at 5.3 m s^{-1} calculated from the intermediate to high RH experiments of Fig. 14; tunnel conditions; ELWC = 0.50 $\pm$ 0.02 g m^{-3}, temperature -16.1 ± 0.6°C. Plotted points are weighted averages of transfers in 2, 3, 8, and 3 experiments, at 3.1, 4.1, 5.3, and 6.1 m s^{-1}, respectively. Note the very large negative charge transfer at 5.3 m s^{-1}.

positive charge transfers in the present study, but they agree well with all three studies when adjusted according to the velocity dependence observed by Keith and Saunders (1990).

The positive charging data suggest that adjustments for the velocity are necessary. However, the present velocity series showed that the maximum negative charge transfer was independent of velocity, except at 5 m s^{-1}. This is contrary to the results of Keith and Saunders (1990), who found that the charge transfer was a strong monotonic function of velocity. They observed that positive charge transfer increased as $V^{2.5}$ at -12°C and negative charge transfer increased as $V^{2.8}$ at -25°C.

7. A conceptual model of thunderstorm electrification

The dominant dependence of the charge transfer on relative humidity may offer insight into the electrification of a thunderstorm by identifying regions of high, low, and intermediate humidities in a simple conceptual model, even if no humidity data are currently available. The region likely to have high RH due to adiabatic cooling is within and directly surrounding the updraft, particularly between cloud base and the -4°C level, where few if any ice crystals are present. Low RH regions would be observed near cloud top due to drying by entrainment and high ice particle concentration. Low RH may also be observed near cloud base in downdrafts and precipitation shafts.

In most of the cloud, droplets and ice crystals coexist for some time, so the nonequilibrium but quasi steady-state RH of the air would depend on the relative number concentration of droplets and ice crystals. Intermediate relative humidities are associated with ice crystal concentrations of the order of 10–100 L^{-1}.

Ice crystals that rise in the updraft would grow rapidly and provide strong negative charge transfers to colliding graupel. The experiments (Fig. 14) showed that the greatest sensitivity to the relative humidity occurs at temperatures between $-13°$ and -18°C, with the strongest negative charge transfers occurring near -15°C. This agrees well with the $-12°$ to -20°C altitude of the first observed negative charge center in thunderstorms.

At the early stages of electrification in a single cell thunderstorm the negative charge center is confined to a small region near the updraft–downdraft transition zone, at altitudes between the $-12°$ and -20°C levels (Dye et al. 1986, 1988). Strong electric field growth, from 100 V to 8 kV m^{-1} in 8 min, is only observed once 5-mm graupel are present (Dye et al. 1986). The requirement of 5-mm graupel in the early negative charge center at or near the -16°C height level before the development of strong electric fields is consistent with the velocity dependence of charging observed at relative humidities near water saturation at -16°C (Fig. 15).

Smaller graupel have lower fall speeds, which are associated with much lower maximum negative charge transfers. Therefore, rapid early electrification may only begin when 5-mm graupel are present in the high humidity updraft region.

This simple model of the relative humidity distribution leads to a conceptual model of single cell thunderstorm electrification (Fig. 19), which may explain several observations that the model of Jayaratne and Saunders (1984) did not. Note that no attempt is made to explain organized multicell, isolated supercell, and multicell airmass thunderstorms, as described extensively by Stolzenfels et al. (1998).

The role of the updraft as a vapor source is also consistent with observations by Williams and Rutledge (1990) that the highest lightning rates observed during an Australian monsoon season corresponded to periods with the highest convective available potential energy (CAPE). Higher CAPE creates stronger updrafts that could raise more moist air, and this seems to be associated with stronger electrification.

The effect of relative humidity can also explain the structure of a mature storm. Using the RH effect, the presence of the negative charge center at altitudes between the $-5°$ and -30°C level can be explained as a

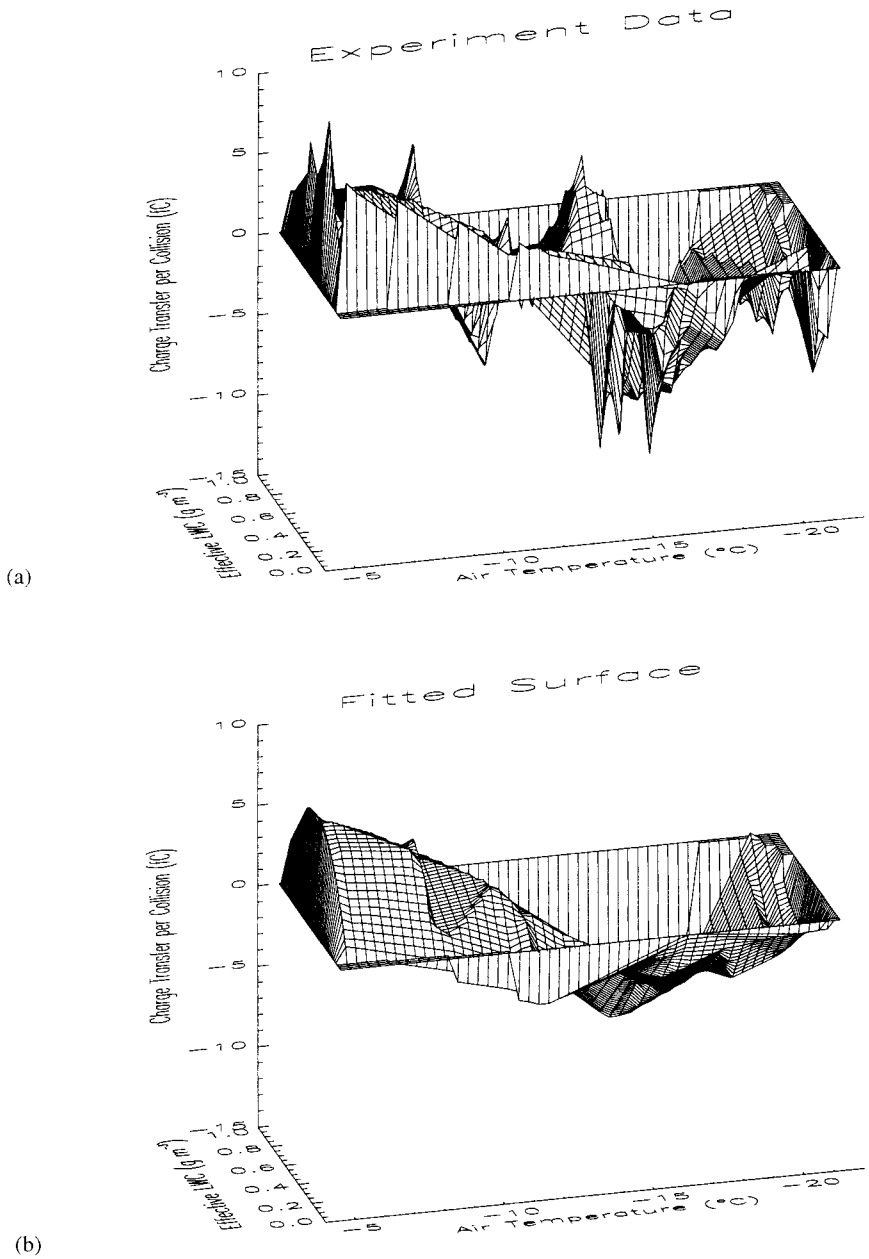

FIG. 16. (a) Plots of charge transfer observed, and (b) charge transfer predicted by Eq. 1, as function of temperature and ELWC.

quasi-static situation. The temperature and ELWC series (Figs. 6–9) showed reversal temperatures between −10° and −14°C for all ELWCs at intermediate relative humidities. This is typically much warmer than the reversal temperatures reported by Jayaratne and Saunders (1984) and corresponds approximately to the temperature at the bottom of the negative charge center. Thus, the charge center may be generated in situ rather than being advected to the observed altitude.

Finally, the existence of the lower positive charge region can be explained by the relative humidity series (Figs. 10–14), which showed that low RH strengthened the positive charge transfer at temperatures warmer than the reversal temperature. If the relative humidity is generally high at low altitudes, pockets of strong positive charge may only develop in regions that have been dried by downdrafts, entrainment, or precipitation shafts. This could explain the local reversal of the electric field below the storm that is associated with the arrival of downdrafts and the corresponding rain gush (Krehbiel 1986).

While this conceptual model offers an explanation for several important phenomena, in situ verification of rel-

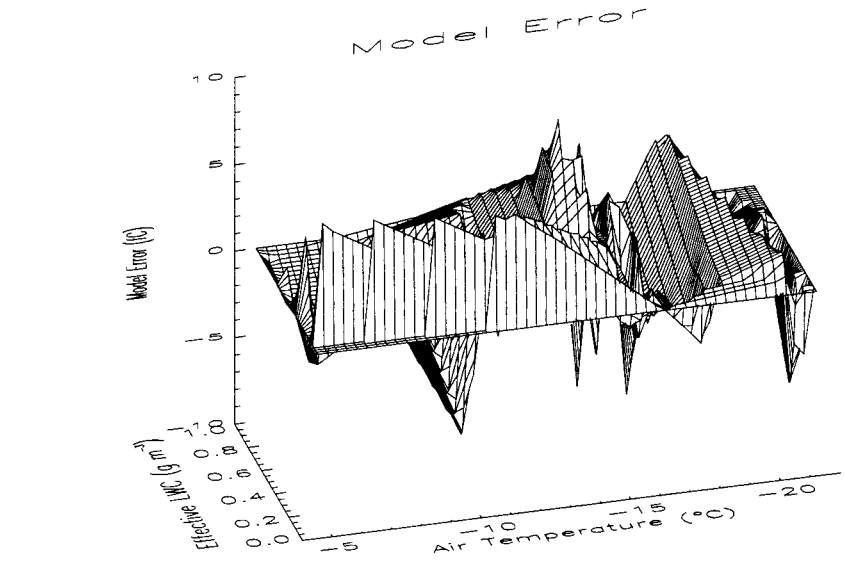

(a)

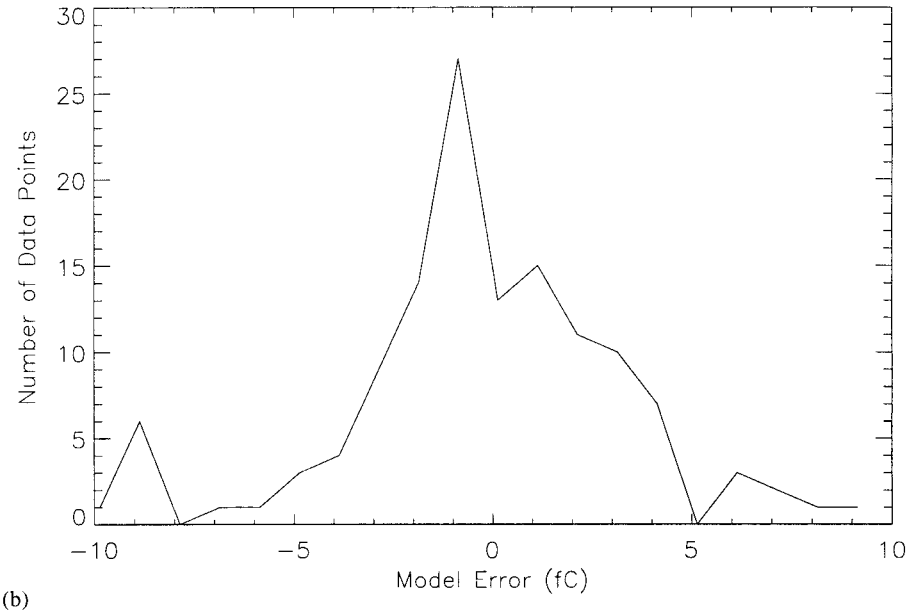

(b)

FIG. 17. Difference between observed charge transfers and model prediction of Eq. (1). (a) Surface plot of difference as function of temperature and ELWC; (b) frequency plot of difference for all 134 data points, plotted in 1-fC intervals.

ative humidity and other cloud physics parameters and by numerical models of the thunderstorm electrification is necessary.

8. Summary and conclusions

The current study provides important insight into the fundamental questions of thunderstorm electrification, both at the scale of cloud particles and, by implication, the thunderstorm as a whole. In addition, the results may offer an explanation for the discrepancies of the previous studies.

The present experiments were performed using a newly developed facility for the study of precipitation particles: the Triple Interaction Facility. It is the first system capable of providing independent control of the solid, liquid, and vapor phases of a simulated cloud. The availability of the facility led to new and mostly unexpected results, revealing several properties of the charge transfer that occurs between colliding graupel

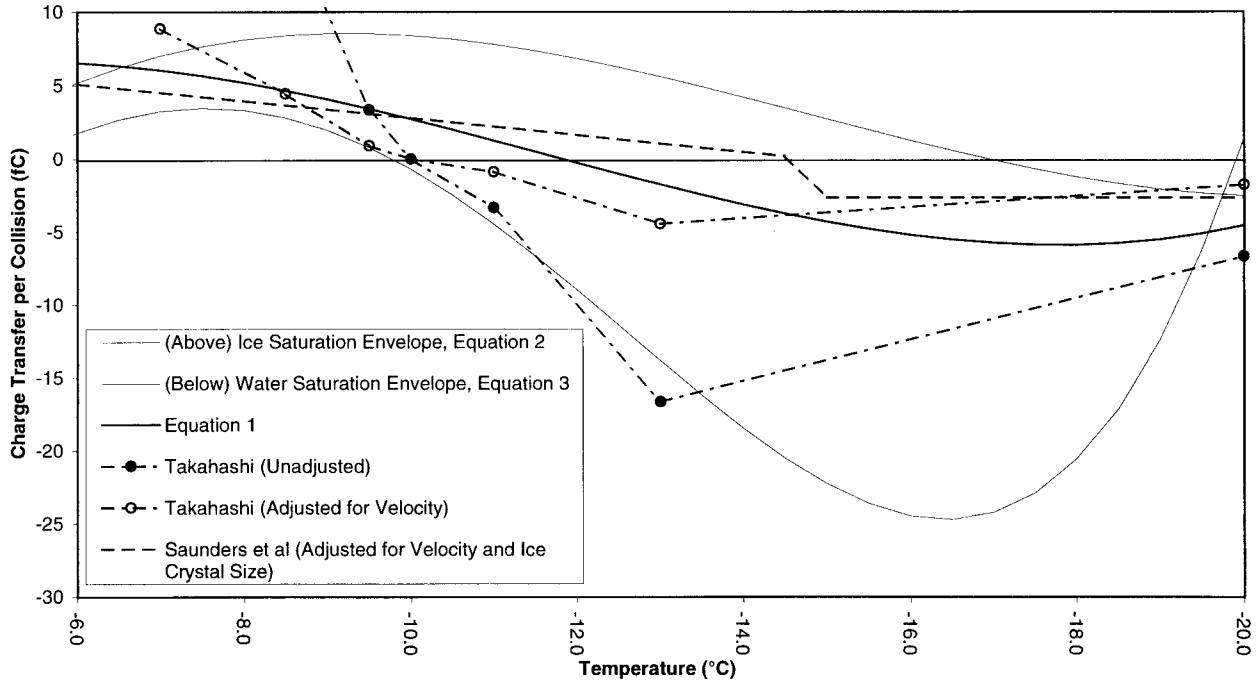

FIG. 18. Comparison of charging observations calculated for ELWC = 0.5 g m^{-3} from Saunders et al. (1991) and Takahashi (1978); envelopes according to Fig. 14. Dash–dot contour lines from Takahashi (1978), assuming LWC = 1 g m^{-3} equals ELWC = 0.5 g m^{-3} with circles as data points. Note Takahashi's (1978) unadjusted maximum C = 33 fC at −6°C (not shown). Thick solid line representing contour surface cut [Eq. (1)].

and ice particles in a cloud of supercooled cloud droplets.

1) This study is the first to observe a strong dependence of the charge transfer on the relative humidity (RH) at which the ice crystals are grown. An increase in RH always favors stronger negative charging, while lowering it promotes weaker negative or stronger positive charging. For a velocity of 5 m s^{-1} this effect was strongest between −13° and −18°C, and varied from +5 and −25 fC per ice crystal collision by increasing the humidity in the ice crystal chamber from ice to water saturation. This is larger than the range observed by varying temperature and ELWC. Near water saturation, charge transfers observed within the first 30–60 s after ice crystal initiation in the chamber were much stronger (>−60 fC per collision near −15°C) than the experiment average of −26 fC.

2) Charging is strongly velocity dependent. At a temperature of −16°C, at high RH, and velocities of 3, 4, and 6 m s^{-1} the maximum average negative charge transfers observed were approximately −5 fC per ice crystal collision, while at ~5 m s^{-1} it was nearly 5 standard deviations apart at −16 fC.

3) Fall speeds of 5 m s^{-1} are associated with ~5-mm graupel at cloud altitudes. This may explain why initial electrification of a thundercloud does not begin until 5-mm graupel are observed (at −16°C, near the temperature of the negative charge center in a thunderstorm).

4) The sign reversal temperature for the charge transfer increased with increasing ELWC, but even more so with increasing ice crystal chamber humidity. In other words, the reversal temperature is not a unique function of the ELWC as previously assumed.

5) The dependence of the reversal temperatures on the RH can explain the controversial results of previous investigations, considering that their results can be fitted within the envelope of charge transfers of the present study.

6) The effect of changes in cloud droplet spectrum on charging was only through ELWC and not the spectra themselves.

7) The best candidates for consistent microphysical mechanisms that explain the newly discovered dependence of the charge transfer on RH are a competition between the negative charge transfer between liquid-like layers on the surfaces of the colliding ice particles and the positive charge transfer due to different dislocation densities.

8) The results of the laboratory experiments have been parameterized for 5 m s^{-1} and are available for sensitivity studies by numerical models of thunderstorms and for the determination of the desirable parameter ranges for future experiments.

9) A simplistic model of thunderstorm electrification, consistent with field observations of single cell thunderstorms and the current laboratory experiments, was offered to explain several localized phenomena including the early electrification in the storm's updraft and the location of the lower positive charge pockets.

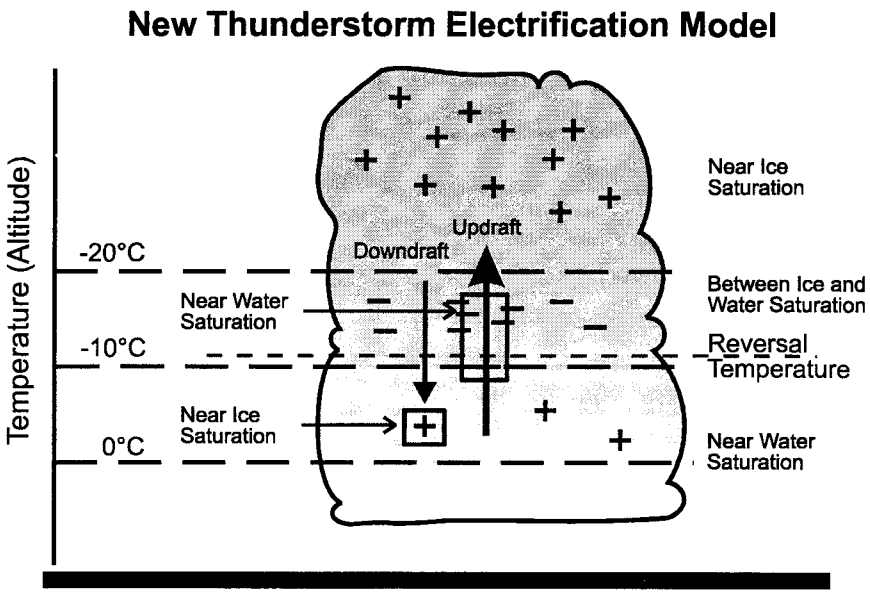

FIG. 19. New conceptual electrification model for single cell thunderstorms, tailored to suggested RH patterns, with main negative charge center developing in situ were highest charging observed in thunderstorms and experiment, in presence of 5-mm graupel. Observed reversal temperature near bottom of negative charge center. Very strong negative charging suggested for region in and around updraft (high RH in rising warm moist air). Positive charge centers at bottom of downdrafts or precipitation shafts due to dry air from above (low RH).

It is recognized that ice particles in a real cloud are created in the same updraft as the graupel that participate in the charge transfer. This means that in future experiments the humidity (and temperature) conditions in the ice crystal chamber need to be set identical to those in the tunnel even if no effect of temperature differences between ICC and tunnel had been found. This could be achieved with better control and measurement of the relative humidity. Such monitoring was not available for the present study because the humidity effect was totally unexpected at the outset of the experiments. However, it was the separation of the ice crystal generation and the graupel growth area that lead to the most important discoveries of this work, and future studies will also require this flexibility.

The effect of atmospheric pressure is another quantity to be explored in charge separation experiments.

The new availability of tunable diode lasers for relatively easy humidity measurement in the laboratory and by storm-penetrating aircraft and balloon should help to answer many of the questions raised in this paper and to better understand thunderstorm electrification.

Acknowledgments. The authors owe special thanks to Drs. S. Cober and P. Joe from the Canadian Atmospheric Environment Service, and Dr. Zheng Guoguang from the Chinese Meteorological Administration. The support by Dr. J. Day from NCAR was particularly appreciated. One of the authors, PB, gratefully acknowledges support through University of Toronto Open Doctoral Fellowships. This study, based on a Ph.D. dissertation of the lead author, was carried out within the research program supported by the National Sciences and Engineering Research Council of Canada and the Canadian Meteorological Service. It represents the report of the last major laboratory study of the Toronto Cloud Physics group. Thus, after 49 years in the field the senior author, RL, wishes to express his sincere thanks to his former 34 Ph.D. and 47 M.Sc. students, supplemented by engineers, technicians, numerous summer students, and post doctorate fellows, who contributed their initiative, intuition, and stealth to the group's overall program and the development leading up to this most challenging undertaking.

Thanks are also given to Dr. C.P.R. Saunders for making his paper, coauthored with his Argentinian colleagues (Pereyra et al. 2000), available to us. In this surprisingly similar paper Berdeklis (1998) was quoted on minor aspects, leaving out his major results and achievements.

REFERENCES

Baker, M. B., and J. G. Dash, 1989: Charge transfer in thunderstorms and the surface melting of ice. *J. Cryst. Growth,* **97,** 770–776.

Berdeklis, P., 1998: The ice crystal–graupel collision charging mechanism of thunderstorm electrification. Ph.D. thesis, University of Toronto, 133 pp.

——, and R. List, 1996: A wind tunnel facility for studying ice crystal–graupel collision charging. Preprints, *10th Int. Conf. on Atmospheric Electricity,* Osaka, Japan, International Commission for Atmospheric Electricity, 18–21.

Brooks, I. M., and C. P. R. Saunders, 1995: Thunderstorm charging: Laboratory experiments clarified. *Atmos. Res.,* **39,** 263–273.

Caranti, J. M., and A. J. I. Illingworth, 1983: The contact potential of rimed ice. *J. Phys. Chem.,* **87,** 4125–4130.
——, E. E. Avila, and R. A. Re, 1991: Charge transfer during individual collisions in ice growing from vapor deposition. *J. Geophys. Res.,* **96,** 15 365–15 375.
Cober, S. G., 1987: Graupel growth in an icing tunnel. M.S. thesis, Department of Physics, University of Toronto, 91 pp.
——, 1991: An experimental investigation of the heat and mass transfer of graupel. Ph.D. thesis, University of Toronto, 149 pp.
——, and R. List, 1993: Measurements of the heat and mass transfer parameters characterizing conical graupel growth. *J. Atmos. Sci.,* **50,** 1591–1609.
Dye, J. E., and Coauthors,1986: Early electrification and precipitation development in a small, isolated Montana cumulonimbus. *J. Geophys. Res.,* **91,** 1231–1247.
——, J. J. Jones, A. J. Weinheimer, and W. P. Winn, 1988: Observations within two regions of charge during initial thunderstorm electrification. *Quart. J. Roy. Meteor. Soc.,* **114,** 1271–1290.
Garcia-Garcia, F., and R. List, 1986: Surface temperature of gyrating hailstone models during accretional growth. Preprints, *Conf. on Cloud Physics*, Vol. 2, Snowmass, CO, Amer. Meteor. Soc., 129–132.
Greenan, B. J. W., and R. List, 1995: Experimental closure of the heat and mass transfer theory of spheroidal hailstones. *J. Atmos. Sci.,* **52,** 3797–3815.
Hallett, J., 1997: The great ice triangle mystery. Preprints, *IAMAS–IAPSO Joint Assemblies*, Melbourne, Australia.
Hanajima, M., 1949: On the growth conditions of man-made snow. *Low Temp. Sci.,* **2,** 23–29.
Hobbs, P. V., 1974: *Ice Physics.* Clarendon Press, 837 pp.
Iribarne, J. V., 1972: The electrical double layer and electrification associated with water disruption processes. *J. Rech. Atmos.,* **6,** 265–281.
——, and M. Klemes, 1974: Electrification associated with droplet production from liquid jets. *J. Chem. Soc., Faraday Trans. I,* **70,** 1219–1227.
Itagaki, K., 1970: X-ray topographic study of vibrating dislocations in ice under an AC electric field. *Adv. X-Ray Anal.,* **13,** 526–538.
——, 1983: Possibility of anomalous relaxation due to the charged dislocation process. *J. Phys. Chem.,* **87,** 4261–4264.
Jayaratne, E. R., and C. P. R. Saunders, 1984: The ''rain gush,'' lightning, and the lower positive charge center in thunderstorms. *J. Geophys. Res.,* **89,** 11 816–11 818.
——, ——, and J. Hallett, 1983: Laboratory studies of the charging of soft-hail during ice crystal interactions. *Quart. J. Roy. Meteor. Soc.,* **109,** 609–630.
Joe, P., and R. List, 1987: Testing and performance of two-dimensional optical array spectrometers with greyscale. *J. Atmos. Oceanic Technol.,* **4,** 139–150.
Keith, W. D., and C. P. R. Saunders, 1988: The collection efficiencies of soft-hailstones for supercooled water droplets and ice crystals. Preprints, *10th Int. Cloud Physics Conf.,* Bad Homburg, Germany, Int. Commission on Cloud Physics, 220–222.
——, and ——, 1990: Further laboratory studies of the charging of graupel during ice crystal interactions. *Atmos. Res.,* **25,** 445–464.
Krehbiel, P. R., 1986: The electrical structure of thunderstorms. *The Earth's Electrical Environment,* National Academy Press, 90–113.
Lesins, G. B., and R. List, 1986: Sponginess and drop shedding of gyrating hailstones in a pressure-controlled icing wind tunnel. *J. Atmos. Sci.,* **43,** 2813–2825.
List, R., and R. S. Schemenauer, 1971: Free-fall behavior of planar snow crystals, conical graupel and small hail. *J. Atmos. Sci.,* **28,** 110–115.
——, G. B. Lesins, F. Garcia-Garcia, and D. B. McDonald, 1987: Pressurized icing tunnel for graupel, hail and secondary raindrop production. *J. Atmos. Oceanic Technol.,* **4,** 454–563.
Locatelli, J. D., and P. V. Hobbs, 1974: Fall speeds and masses of solid precipitation particles. *J. Geophys. Res.,* **79,** 2185–2197.
Mandel, J., 1964: *The Statistical Analysis of Experimental Data.* Dover Publications, 410 pp.
Mason, B. J., 1988: The generation of electric charges and fields in thunderstorms. *Proc. Roy. Soc. London,* **415,** 303–315.
May, K. R., 1950: The measurement of airborne droplets by the magnesium oxide method. *J. Sci. Instrum.,* **27,** 128–130.
Pereyra, R. G., E. E. Avila, N. E. Castellano, and C. P. R. Saunders, 2000: A laboratory study of graupel charging. *J. Geophys. Res.,* **105** (D16), 20 804–20 812.
Press, W. H., S. A. Teukolsky, W. T. Vettering, and B. P. Flannery, 1992: *Numerical Recipes in C: The Art of Scientific Computing.* 2d ed. Cambridge University Press, 994 pp.
Reynolds, S. E., M. Brook, and M. F. Gourley, 1957: Thunderstorm charge separation. *J. Meteor.,* **14,** 426–436.
Saunders, C. P. R., 1993: A review of thunderstorm electrification processes. *J. Appl. Meteor.,* **32,** 642–655.
——, 1995: Thunderstorm electrification. Vol. 1, *Handbook of Atmospheric Electrodynamics*, Hans Volland, Ed., CRC Press, 61–92.
——, W. D. Keith, and R. P. Mitzeva, 1991: The effect of liquid water on thunderstorm charging. *J. Geophys. Res.,* **96,** 11 007–11 017.
Stolzenfels, M., W. D. Rust, and T. C. Marshall, 1998: Electrical structure in thunderstorm convective regions. Part 3: Synthesis. *J. Geophys. Res.,* **103** (D12), 14 097–14 108.
Takahashi, T., 1978: Riming electrification as a charge generation mechanism in thunderstorms. *J. Atmos. Sci.,* **35,** 1536–1548.
——, 1986: Reversal of the sign of the charge on graupel during riming electrification measurements in Hokuriku winter clouds and in a wind tunnel. *Proc. 11th Int. Conf. on Atmospheric Electricity,* Huntsville, AL, International Commission of Atmospheric Electricity, 304–307.
——, and N. Fukuta, 1988: Ice crystal replication with common plastic solutions. *J. Atmos. Oceanic Technol.,* **5,** 129–135.
——, T. Endoh, G. Wakahama, and N. Fukuta, 1990: Vapor diffusional growth of free-falling snow crystals between −3° and −23°C. *J. Meteor. Soc. Japan,* **69,** 15–30.
Vonnegut, B., D. J. Latham, C. B. Moore, and S. J. Hunyady, 1995: An explanation for anomalous lightning from forest fire clouds. *J. Geophys. Res.,* **100,** 5037–5050.
Williams, E. R., and S. A. Rutledge, 1990: Studies of electrification and lightning in deep tropical precipitation systems. *Proc. 12th Int. Conf. on Cloud Physics,* Zurich, Switzerland, International Commission for Clouds and Preciptitation, 290–294.
Zheng, G., and R. List, 1996: Convective heat transfer of rotating spheres and spheroids with non-homogenous surface temperatures. *Int. J. Heat Mass Transfer,* **39,** 1815–1826.